Solution Studies of Xanthan Gum Employing Quasielastic Light Scattering

J. G. Southwick, M. E. McDonnell, A. M. Jamieson, and J. Blackwell*

Department of Macromolecular Science, Case Western Reserve University, Cleveland, Ohio 44106. *Received July 3, 1978*

ABSTRACT: We have used quasi-elastic light scattering, circular dichroism spectroscopy, and viscosity measurements to investigate the thermal transition reported to occur for xanthan in aqueous solution at low ionic strength. The light-scattering data indicate that the diffusion coefficient of the macromolecule significantly increases with increasing temperature in the vicinity of the transition temperature. In addition there is an increase in macromolecular polydispersity near to the transition temperature. These observations suggest that the transition involves the breakdown of a multimolecular aggregate. Translational diffusion coefficients estimated from the light-scattering data for xanthan in low ionic strength solutions show different behavior in two concentration ranges, corresponding to dilute and entangled solutions. For the dilute solution range, extrapolation to zero concentration yields a z-average translational diffusion coefficient $D_T^\circ = 1.66 \times 10^{-8}$ cm^2/s at 25 °C which corresponds to a z-average hydrodynamic radius of 146 nm obtained using the Stokes–Einstein equation. The variation of the diffusion coefficient with concentration in the region where chain entanglements are expected does not agree with recent theoretical predictions on solution behavior under these conditions. An explanation of this discrepancy is proposed based on the high chain stiffness inherent in the xanthan molecule.

The extracellular polysaccharide produced by the bacterium *Xanthomonas campestris*, commonly referred to as xanthan gum, has been found to possess commercially useful physical properties. Xanthan gum functions as a viscosity enhancing agent in a wide variety of food products. Solutions of xanthan gum have been shown to maintain high viscosity over a wide range of salt concentration, pH, and temperature, and the viscosity is also insensitive to the electrolyte species present.[1] However, the viscosity of a xanthan solution is very sensitive to shear: with increasing rate of shear the viscosity decreases rapidly, but is immediately recoverable when the shearing force is removed. These properties are highly desirable in tertiary oil recovery solutions, and thus xanthan has potential applications in this area. Although xanthan solutions have been characterized extensively, an understanding of the molecular interactions giving rise to these properties is for the most part still lacking.

Xanthan gum[2,3] is a polysaccharide possessing extensive short-chain branching; the chemical structure is shown in Figure 1. The backbone is a cellulose chain (poly[β-(1→4)-D-glucose]), and every second backbone residue has a β(1→3) substituted trisaccharide side chain (β-D-mannopyranosyl-(1→4)-α-D-glucuropyranosyl-(1→2)-β-D-mannopyranoside 6-*O*-acetate). In addition the terminal D-mannose residue of the side chain may have a pyruvic acid residue linked to the 4- and 6-positions. The degree of pyruvate substitution is typically in the range from 25–50% and it has been shown that this is an important parameter affecting the physical properties of xanthan solutions.[4] At present it is uncertain whether the pyruvic acid residues are distributed in blocks along the chain or whether their substitution is random.

A combined X-ray diffraction and stereochemical packing study[5] has determined that the most probable model for xanthan is a 5_1 right-handed helix repeating in 47 Å. A significant feature of the proposed structure is that the trisaccharide side chains are arranged close to the helical backbone, to which they are hydrogen bonded. Xanthan is difficult to crystallize and the diffraction patterns were not sufficiently well resolved to permit more definite conclusions. The model proposed was only the most probable one based on energetic considerations and the study stresses that multistranded structures are consistent with the X-ray data and represent alternative conformations.

Xanthan solutions at low ionic strength have been shown to undergo a thermal transition, which has been detected by a number of physical methods: viscosity,[1] optical rotation,[6] NMR spectroscopy,[6] and circular dichroism spectroscopy.[6] The transition was first detected as a sigmoidal increase in the viscosity of 1% salt-free solutions with midpoint at ~55 °C.[1] Subsequent spectroscopic studies have detected transitions coincident with the change in viscosity suggesting that this change is due to a conformational transition of the molecule. At room temperature, a broad, featureless NMR spectrum is obtained, suggesting a high degree of order in the system. Above the transition temperature sharper spectra are obtained, indicative of a loss of order. As a result the transition has been explained as a helix to flexible coil transition, perhaps with the coil form having the trisaccharide side chains oriented away from the main chain and into the solvent.

More recently electron microscopy[7] studies have produced evidence suggesting that xanthan has a multistranded helical conformation. The undenatured native xanthan molecule appeared as an unbranched fiber 4 nm wide and 2–10 μm long, compared to strands 2 nm wide and 0.3–1.8 μm long seen for the denatured form. Upon renaturation the fiber dimensions were once again 4 nm wide, 2–10 μm long, but the micrographs showed numerous regions in which the native assembly was partly unraveled. In view of the twofold reduction in fiber diameter a double helix model seemed most likely, but other multistranded helices were still considered possible. Estimates of the molecular weight of xanthan in the native and denatured states led to the conclusion that the native molecule is assembled from approximately 40 single chains. Additional evidence supporting the multistranded conformation for xanthan stems from similarities which exist between the thermal transition observed for xanthan solutions and the melting of double helical DNA.[8] In particular it has been pointed out that for both xanthan and DNA the following similarities exist: (1) the charged groups are further apart in the denatured form than in the native conformation; (2) the transition breadth is increased upon the addition of divalent salts; (3) there is a linear dependence of the

0024-9297/79/2212-0305$01.00/0

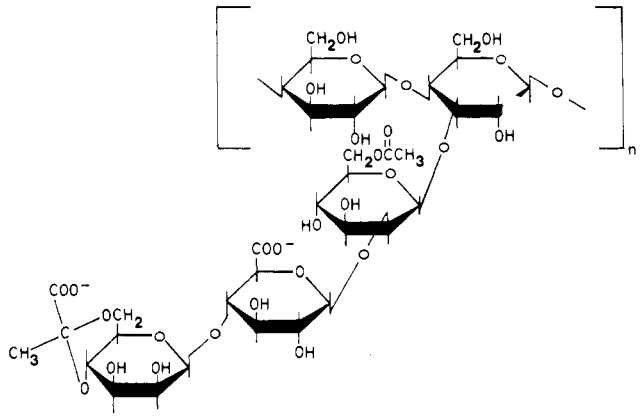

Figure 1. Structural formula for the repeating unit of xanthan gum.

melting transition temperature on the logarithm of the counterion activity; and (4) renaturation is dependent on the ionic environment.

In the work described below our aim has been to confirm the observations of other groups concerning the temperature transition in xanthan solutions and then to apply quasielastic light scattering to investigate the changes in chain dimensions caused by the transition.

Quasielastic Light Scattering

Quasielastic light scattering is a technique allowing the rapid determination of macromolecular diffusion coefficients, which can then be related to the dimensions and interactions of macromolecules in solution. Dynamic light scattering as applied in our experiments analyzes the frequency distribution of intensity fluctuations of monochromatic incident radiation resulting from motion of the scattering species. The frequency distribution may arise from several effects including translational diffusion, rotational diffusion, and internal relaxations. We have applied dynamic light scattering to the study of xanthan solutions in order to determine the translational diffusion coefficient as a function of temperature, and through the Stokes–Einstein equation:

$$D_0 = kT/6\pi\eta R_h \qquad (1)$$

to relate the diffusion coefficients to the hydrodynamic radius of the molecule. It is to be expected that the transition will manifest itself as a change in the hydrodynamic radius from which a relative change in molecular weight can also be estimated. In the case of xanthan, experimental and theoretical difficulties exist in determining the translational diffusion coefficient due to the low intensity of scattered light, high molecular weight, sample polydispersity, and the fact that the thermally induced transition occurs only in solutions of low ionic strength, where charge repulsions between xanthan molecules become a significant factor affecting diffusion.

Since the measurement of translational diffusion in xanthan solutions is sought, it is important to be certain that the spectrum does not contain components arising from intramolecular relaxations. This is accomplished by experimentally determining the range of angles over which the following relationship holds:

$$\Gamma = D_T K^2 \qquad (2)$$

where Γ is the half-width at half-height of the spectrum and K is the scattering vector. Above a critical scattering angle internal relaxations will contribute to the spectrum and the half-width will be wider than that predicted by eq 2. It is predicted that internal effects will be detected at scattering angles for which $KL \gg 1$, where L is the largest dimension of the macromolecule.

Experimental Section

Preparation of Solutions. Samples of xanthan were kindly supplied by Dr. Paul Sanford, Department of Agriculture, Northern Regional Research Laboratory, and were in the form of a purified, freeze-dried white powder. Aqueous solutions of xanthan were prepared by addition of deionized water, dialyzing for 3 days against deionized water, and filtering through 0.8μm Millipore filters. In order to study the effect of concentration on viscosity and diffusion at low ionic strength the ionic strength was kept approximately constant to avoid charge sensitive conformational transitions which occur for many polyelectrolytes.[9] We assumed the existence of one mobile counterion for each charged group on xanthan, and also the pyruvic acid residues were present on 37% of the xanthan side chains, which allowed a direct calculation of the change in ionic strength of the solution resulting from the change in xanthan concentration. Small amounts of NaCl were then added to the diluted solution to restore the original ionic strength.

Viscosity Measurements. Ostwald-Fenke viscometers were used to determine the viscosities of xanthan solutions prepared at concentrations of 1% in distilled water and 0.5% in 0.5% aqueous KCl. The 1% xanthan solutions in 0.5% KCl were too viscous for flow measurements, but it has been shown that this dilution does not alter the trend of the viscosity–temperature relationship.[1] Viscosity measurements of more dilute xanthan solutions ($\leq$0.1%) were performed using a No. 50 Cannon-Ubbelhode viscometer. The temperatures were controlled using a Haake E-52 water bath circulator.

Circular Dichroism. Circular dichroism spectra were recorded using a Jasco J20 spectropolarimeter equipped with a jacketed 2 mm quartz cell. Temperature control was achieved using a Neslab T3 circulating water bath with a refrigeration unit to control temperatures below 35 °C. The spectra were recorded several times at each temperature to ensure that equilibrium had been attained. The CD data are reported as molar ellipticity [θ] in units of deg cm^2 dmol^{-1} based on the average molecular weight of a single saccharide residue.

Quasielastic Light Scattering. The laser light scattering instrument consists of a Coherent Radiation Model 52B argon ion laser, an EMI 9656 KR phototube, a Keithley 104 wide band amplifier, and a Saicor SA 1-52 real time 400 point spectrum analyzer and digital integrator. Homodyne spectra were recorded as voltage spectra rather than power spectra, since the spectrum analyzer processes the former more accurately. Power spectra were then obtained by squaring 40 data points of the voltage spectrum and subtracting the square of the baseline intensity. These data formed the input for a Lorentzian curve fitting program, from which the half-width at half-height was determined. Solutions contained in a small Pyrex tube were placed in a bath of decahydronaphthalene, which has approximately the same refractive index as glass. This reduces the intensity of the elastically scattered light at the cell surface and allows a true homodyne spectrum to be recorded.

The low intensity of the light scattered by xanthan solutions created a problem in that parasitic scattering from microscopic dust particles could be significant. In order to minimize this problem, the solutions were centrifuged for 30 min in the scattering cell at 6000 rpm before collecting data. Solutions prepared in this manner displayed no more than 5% fluctuation in the dc voltage from the photomultiplier tube.

Samples of xanthan are polydisperse: typically $M_w/M_n \sim 2.8$.[10] While it is not expected that the spectra for polydisperse samples such as this will fit a single Lorentzian curve with a high degree of precision, one can see from Figure 2 that the data are nearly Lorentzian, and by disregarding the first two low-frequency data points a good fit of the experimental data to a single Lorentzian is attained. Once a good fit of the data to a single Lorentzian has been attained, disregarding additional low-frequency data points only slightly changes the measured half-width. We interpret this uncertainty to be due to experimental errors and have calculated error bars in accordance with this observation for Figure 9. Neglecting low-frequency data until a constant half-width is attained corresponds to determining the diffusion coefficient

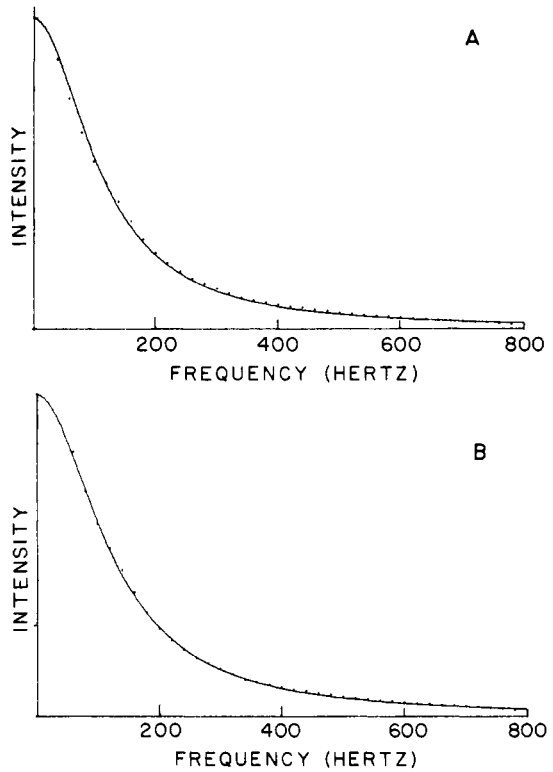

Figure 2. Experimental data points from a quasielastic light scattering spectrum of a salt-free 0.1% xanthan solution at 22 °C along with the best least-squares fit of a Lorentzian curve to these points: (A) all data points included; (B) the first two low-frequency data points have been skipped.

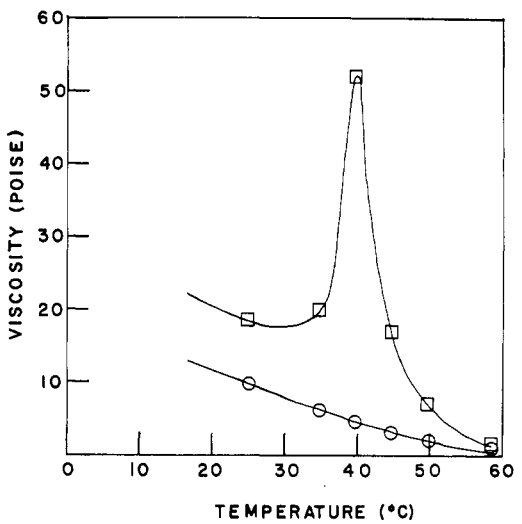

Figure 3. Viscosities of xanthan solutions plotted as a function of temperature: (□) salt-free 1% xanthan solution; (○) 0.5% xanthan in 0.5% KCl solution.

associated with the high-frequency limit, which has been shown[11] to be equivalent to the initial slope of the autocorrelation function of the photocurrent. Ford et al.[12] have related this initial slope to the z-average diffusion coefficient of the distribution for cases where internal interference is absent. All our half-widths have been determined via this method, so our values determined at low scattering angles ($\theta < 50°$) correspond to the z-average diffusion coefficient of the molecular weight distribution. Typically, 2 of the 40 data points were neglected.

Results

Viscosity. In Figure 3 it is seen that 1% salt-free solutions show a sharp increase in viscosity between 35 and 40 °C, and these results match the observations by other

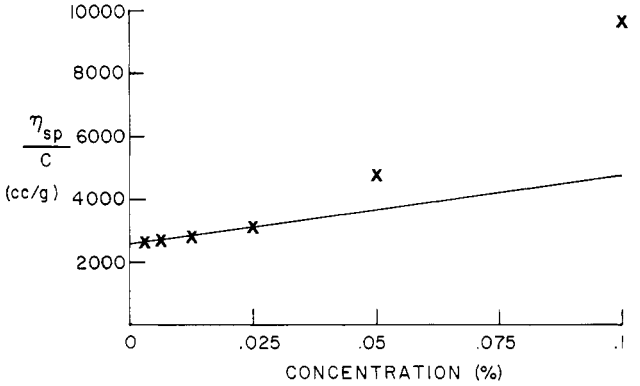

Figure 4. Plot of specific viscosity/concentration against concentration for low ionic strength xanthan solutions at 25 °C.

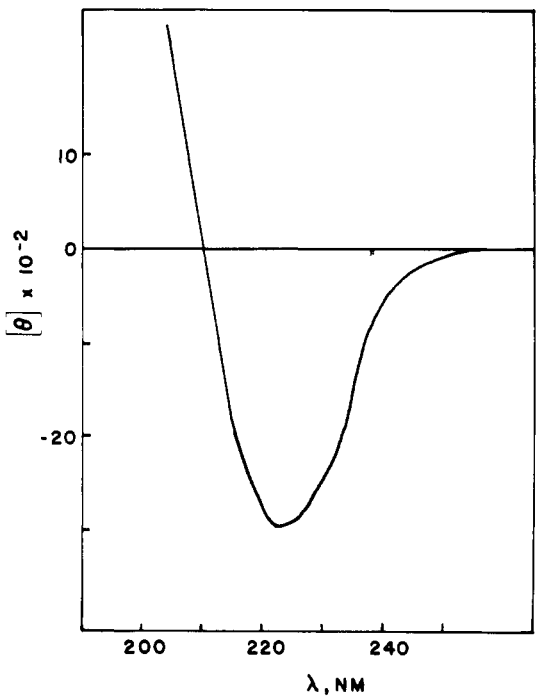

Figure 5. Circular dichroism of a salt-free 0.2% xanthan solution at 22 °C.

workers. However, xanthan solutions containing 0.5% KCl show no sharp transition in viscosity. Shear rates ranged from 0.61 to 20.9 s^{-1} for salt-free xanthan solutions, and from 3.8 to 30.6 s^{-1} for xanthan solutions containing 0.5% KCl. Figure 4 shows the specific viscosity/concentration of xanthan plotted against concentration for low ionic strength solutions. It is seen that a linear plot of η_{sp}/c vs. c is obtained to a concentration of 0.025%; higher concentrations result in viscosities above those predicted by a linear relationship. Shear rates in these measurements varied from 144 s^{-1} at the lowest concentration to 14.5 s^{-1} at 0.1%. Although xanthan solutions exhibit shear thinning behavior, a similar transition above 0.03% concentration is evidenced in viscometric data extrapolated to zero shear.[13] This indicates that chain entanglements are the likely cause of the high viscosities measured at concentrations above 0.025%.

Circular Dichroism. The circular dichroism spectrum of a salt-free 0.2% xanthan solution at 22 °C is shown in Figure 5. The spectrum has a trough at 222 nm and a peak at approximately 200 nm; the latter is difficult to resolve due to instrumental limitations. The trough at 222 nm is at a typical wavelength for the n–π* transition of a carboxylate ester, and this band can be assigned to the

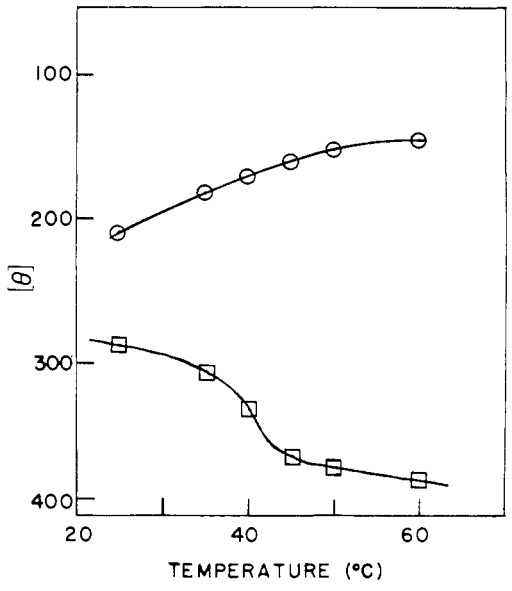

Figure 6. Ellipticity of xanthan at the minimum (215–220 nm) plotted as a function of temperature: (□) salt-free 0.2% xanthan solution; (○) 0.2% xanthan in 0.5% KCl solution.

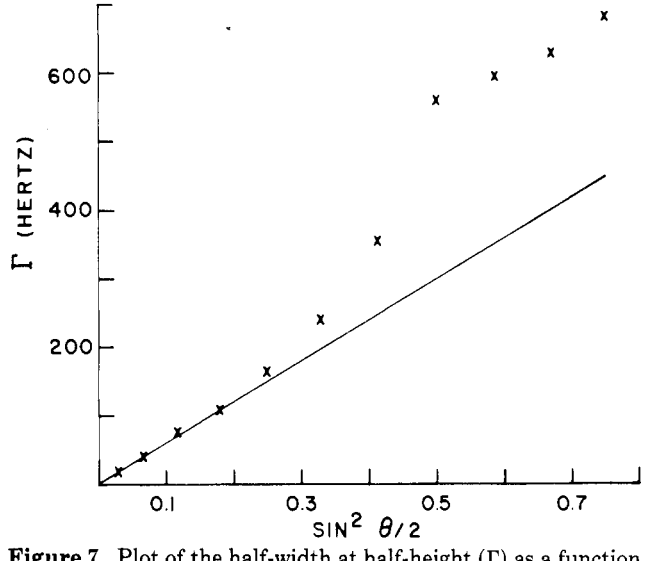

Figure 7. Plot of the half-width at half-height (Γ) as a function of scattering angle ($\sin^2 \theta/2$) for a 0.025% salt-free solution of xanthan at 25 °C.

O-acetyl group.[6] Figure 6 shows the temperature dependence of the 222-nm band for both salt-free solutions and solutions containing 0.5% KCl. For the salt-free solutions the ellipticity decreases sigmoidally as the temperature increases with midpoint for the transition at 40 °C. The results are indicative of a conformational transition and suggest that this involves a change in the environment of the acetate groups. In contrast, the solutions containing KCl display an almost linear increase in ellipticity.

Quasielastic Light Scattering. Half-widths determined for the light scattering spectra of 0.025% and 0.1% salt-free xanthan solutions as a function of scattering angle are shown in Figures 7 and 8, respectively. Both plots show a linear relationship between Γ and $\sin^2 \theta/2$ for $\theta < 50°$; as a result a scattering angle of 40° was used for measuring translational diffusion in these systems. Fewer deviations from linearity between the measured half-width and $\sin^2 \theta/2$ are seen for the more concentrated solution.

The ionic strengths of the solutions were kept approximately constant in order to study the effect of

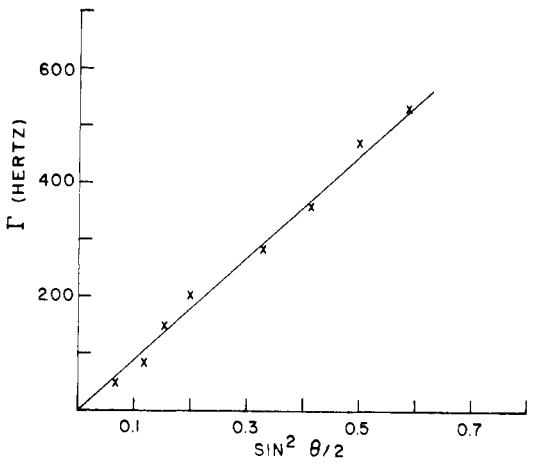

Figure 8. Plot of the half-width at half-height (Γ) as a function of scattering angle ($\sin^2 \theta/2$) for a 0.1% salt-free solution of xanthan at 25 °C.

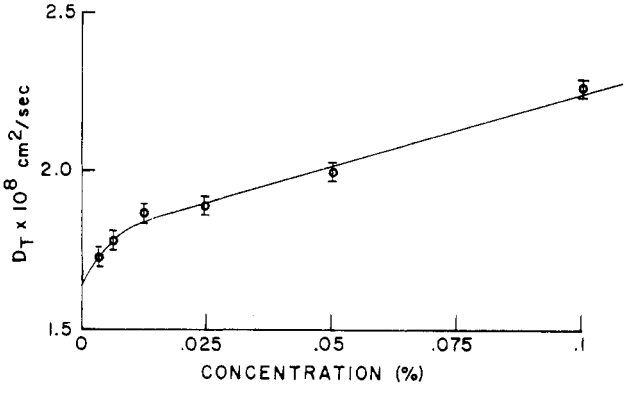

Figure 9. Translational diffusion coefficients plotted against concentration for low ionic strength xanthan solutions. Data were collected at a scattering angle of 40 °C at 25 °C.

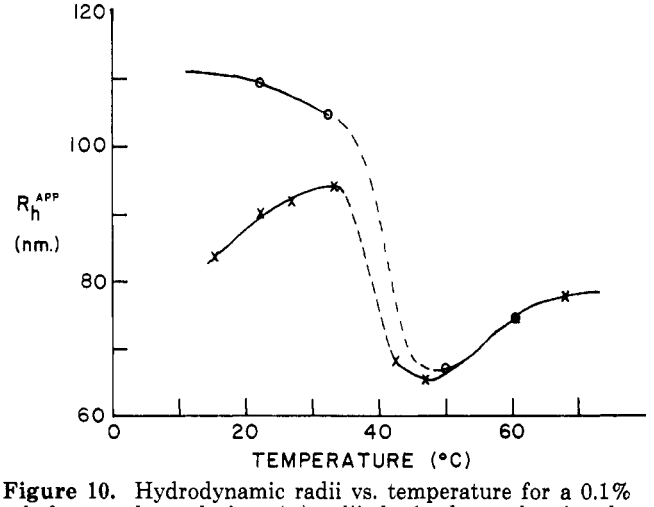

Figure 10. Hydrodynamic radii vs. temperature for a 0.1% salt-free xanthan solution: (×) radii obtained upon heating the solution; (○) radii obtained upon cooling. Broken lines correspond to temperatures where z-average diffusion coefficients could not be determined due to polydispersity.

concentration on translational diffusion. In Figure 9 translational diffusion coefficients are shown for xanthan solutions of differing concentrations at low ionic strength. It is seen that D_T increases rapidly up to a concentration of 0.0125%, whereupon a more gradual increase of D_T with concentration occurs between 0.0125 and 0.1%. Extrapolation to zero concentration yields a $D_T^0 = 1.66 \times 10^{-8}$ cm²/s, from which a hydrodynamic radius (R_h) of 146 nm is calculated.

Table I
Radii Plotted with Points Skipped

temp, °C	R_h, A	points skipped
15.9	842	2
22.3	905	2
27.3	920	2
33.2	938	3
35.5		do not converge
37.1		
42.3	681	10
46.7	652	8
52.6	682	8
60.2	747	5
68	771	5
60.2	746	5
50	671	8
39.5		does not converge
32.3	1040	2
22.7	1094	2

Figure 10 shows the hydrodynamic radii determined from the Stokes–Einstein equation plotted as a function of temperature for a 0.1% salt-free xanthan solution. The significance of R_h^{app} will be discussed below. It is seen that heating the solution results in an increase in R_h^{app} from 840 Å at 15 °C to 940 Å at 34 °C, whereupon a further increase in temperature causes the measured radius to decline to 650 Å at ~47 °C. Above 47 °C the macromolecular dimensions again increase with temperature to a value of 770 Å at ~68 °C. Upon cooling the solution a sigmoidal increase in the hydrodynamic radius was seen, with midpoint ~39 °C, and the radius measured at room temperature (22 °C) after heating and cooling is ~1100 Å, which is ~200 Å larger than the original value (i.e., before heating).

The number of experimental data points which had to be neglected before a good fit of the remaining points to a single Lorentzian curve was found to be temperature dependent. Table I presents the experimental temperatures, hydrodynamic radii, and the number of neglected data points. Below the transition temperature (38 °C) neglecting two points resulted in a good fit to a Lorentzian curve, whereas at temperatures well above the transition (>60 °C) five points must be neglected to obtain the same degree of fit. Experimental spectra obtained in the region of the transition (35–40 °C) could not be fitted to a Lorentzian curve regardless of the number of points skipped, and therefore z-average hydrodynamic radii could not be determined at these temperatures.

Discussion

Effect of Concentration. The range of concentrations studied in Figures 4 and 9 includes both dilute solutions of xanthan and concentrations where considerable molecular overlap is expected. An approximate picture of the molecular arrangement in solutions can be produced by calculating the average interparticle distance. If it is assumed that the average shape of xanthan in solution is spherical, then the average volume available to each particle is $V = 1/p$, where p is the number of molecules per unit volume and can be calculated from the concentration and molecular weight. In turn by assuming these volumes are spheres, the average radius of influence (R) can be estimated. Therefore the mean interparticle distance d is equal to $(R - R_g)$, where R_g is related to our experimentally determined value for R_h of 146 nm, by $R_g = 1.51R_h$.[14] Table II shows the interparticle distances calculated for various concentrations. A dilute solution can be defined as one in which the polymer molecules are separated by at least one molecular diameter,[15] which

Table II

concn, %	mean interparticle distance, A
0.003125	5290
0.00625	3290
0.0125	1710
0.025	430
0.05	overlapped
0.1	overlapped

corresponds to approximately 10% occupancy by the polymer spheres. On this basis, a dilute xanthan solution occurs for concentrations $c < 0.1M(4/3)\pi R_h^3 N_o$ where M is the molecular weight and N_o is Avogadro's number. The molecular weight of a similar xanthan sample was estimated by Holzwarth using sedimentation analysis[10] to be $M_w = 9.0 \times 10^6$ D. Using this value with our determined R_h = 146 nm we arrive at a limiting concentration of 0.0115%. Thus, the slope of the curve in Figure 8 in the concentration range zero to 0.0125% describes the behavior of xanthan in dilute solution. The linear increase in D_T with increasing concentration is explained by the effect of charge–charge repulsions on the polymer molecules.[16]

At concentrations above 0.0125%, D_T once again increases with concentration, albeit at a slower rate than in the dilute solution range. It seems from the data that this region of concentration (0.0125–0.1%) corresponds to another solution condition, where chain entanglements are becoming an important factor affecting diffusion. Our interpretation that chain entanglements are present in this concentration range is supported by the calculations presented in Table II. It is seen that predicted chain overlap due to space restrictions occurs at roughly 0.05%. This calculation does not correlate quantitatively with our observed concentration transition above 0.0125%; however, there are several reasons to believe that entanglements will occur at concentrations below those predicted. The calculation is based on a time-averaged spherical model, and does not take into account that the instantaneous shape of a flexible polymer coil is nonspherical, as shown by Kuhn,[17] and subsequently Solc and Stockmayer.[18,19] Also the chain stiffness of xanthan can enhance the anisometric shape in solution. Further indications of chain entanglements at concentrations in this range are seen in the transition in the concentration dependence of the viscosity data (Figure 4), the viscosity data of the other workers,[13] and the angular dependence of scattered light. Network-type oscillations which are expected for entangled systems are known to produce half-widths (Γ) proportional to K^2.[20] It is seen in Figures 7 and 8 that the half-width is much more nearly proportional to K^2 for low ionic strength solutions at a concentration of 0.1% than for 0.025% solutions. This suggests the presence of network oscillations, and thus entanglements, at 0.1% concentration.

Recent theoretical developments[21–23] dealing with the behavior of entangled polymeric solutions have modeled these solutions as "temporary networks". Under these conditions, diffusion of the center of mass of a molecule is no longer possible since the steric restrictions allow only the diffusion of chain *segments* between entanglement points. The concentration dependence of the measured diffusion is explained by the fact that the introduction of entanglements effectively reduces the molecular weight of the diffusing component, hence increasing D_T. The diffusion coefficient according to deGennes' theory[23] is proportional to K^2 and $C^{0.75}$ and significantly does not depend on molecular weight.

An important consideration is that one can only expect

to detect these network oscillations at certain scattering angles, the requirement being that the characteristic fluctation frequency is higher than the frequency of the formation and breakdown of the contact points.[20] This condition corresponds to the existence of a critical scattering angle θ_{CR}, below which network oscillations are not detected. The value of θ_{CR} is dependent on the hydrodynamic radius of the macromolecule and the concentration of the solution. The largest θ_{CR} value possible for a given hydrodynamic radius occurs at the concentration where molecular overlaps begin to occur (c^*). For xanthan the maximum value θ_{CR} can assume is 23°, and consequently our experimental scattering angle of 40° is expected to detect network oscillations.

Our results show the expected increase in diffusion with concentration, but this increase is not nearly as large as predicted by deGennes'[23] theory. The diffusion coefficient is proportional to $C^{0.143}$ for concentrations between 0.025 and 0.1%. We are aware of recent data for polystyrene solutions[20] which predict a $C^{0.67}$ dependence for Γ (i.e., almost theoretical behavior), and the discrepancy in our case is probably related to the stiffness of the xanthan chains. Stiff chains are not expected to allow as many molecular entanglements as flexible coils at a given concentration. While deGennes' theory is only rigorous for flexible coils, effects of stiffness may be accounted for in principle. If we assume a rigid rod for xanthan ($\nu = 1.0$) then the reduction in the chain length between entanglements is expected to scale as $C^{0.5}$ rather than $C^{0.75}$, which is still inconsistent with our experimental results. A further effect of xanthan chain stiffness is that if the persistence length of the macromolecule is the same order of magnitude as the chain length between entanglement points (ξ), the assumption that these chain lengths exhibit unrestricted diffusion becomes inadmissible. While there have been no reported values for the persistence length of xanthan, similarities in solution behavior between xanthan and DNA suggest that it is reasonable to assume that the persistence length of xanthan is of the order of 100 nm. A persistence length of this magnitude is comparable to the Stokes radius of the molecule and will therefore be comparable to ξ even at the critical concentration (c^*), since ξ decreases with increasing concentration. One might expect to see a second discrete transition in the concentration dependence of D_T when the persistence length becomes greater than the correlation length. We have obtained preliminary data which tend to confirm this speculation and are planning additional experiments to investigate this area.

Temperature Transition

We have shown that quasielastic light scattering can be used to follow the thermal transition in xanthan solutions. Since the same transition temperatures were determined using viscosity, circular dichroism, and quasielastic light scattering measurements, the results indicate the transition temperature is not dependent upon the concentration of polysaccharide. Our observation of the transition at ~38 °C does not match the temperature of 55 °C reported by other workers.[1,6] However, more recent evidence[8] shows that the transition temperature is particularly sensitive to traces of undialyzed electrolyte in the solution.

In our light scattering experiments, the fact that data were collected from semidilute solutions poses an interpretative problem. In Figure 10, we observe that R_h^{app} exhibits a sigmoidal decrease through the transition. However, R_h^{app} does not bear a simple relationship to the true Stokes radius measured at infinite dilution. We can utilize the theoretical relationship derived by deGennes[23] for the mutual diffusion coefficient of semidilute polymer solutions

$$D_c = kTB/c\xi^3 \tag{3}$$

where B is the frictional mobility of a monomer segment and ξ is the concentration-dependent correlation length for entanglements. The decrease in R_h^{app} at the thermal transition in xanthan is then seen to be in accord with two events which would accompany a helix-to-coil transition in an entangled polymer solution: an increase in segmental mobility, and a decrease in ξ. However, the decrease of ~30% in the R_h^{app} observed during the transition does not seem compatible with a 40-fold reduction in molecular weight proposed by other workers, which would predict a reduction in hydrodynamic radius of ~90%.

Table I indicates that there is a poorer fit to a single Lorentzian curve at and above the transition than there is at low temperature. This poor fit could be due to polydispersity, or to the presence of additional relaxation modes in the light scattering spectrum. Since we are observing predominantly the isotropic scattering component, the latter explanation seems unlikely. Consequently polydispersity of the diffusional relaxation appears to be the only reasonable explanation for the behavior in Table I. Thus, the polydispersity of the diffusional relaxation becomes extremely large in the region of the transition and above the transition remains higher than the original polydispersity. For single helix → random coil structures, single relaxation behavior has been reported through the transition region.[24,25] We therefore feel that the observed polydispersity in the relaxation times for xanthan is an indication that the transition occurs through a multistranded → subunit model.[7] To test this hypothesis, further studies are underway utilizing photon correlation spectroscopy, so more quantitative information can be attained concerning the denatured state of xanthan.

Acknowledgment. The authors wish to thank Dr. Paul Sanford for providing us with samples of xanthan. We also wish to thank Dr. George Holzwarth for helpful discussions, for determining molecular weights, and for obtaining zero shear intrinsic viscosities of our samples. This research is supported by N.S.F. Grant No. PCM18631 and ENG. 76-20278.

References and Notes

(1) A. Jeanes, J. E. Pittsley, and F. R. Senti, *J. Appl. Polym. Sci.*, **5**, 519 (1961).
(2) P. E. Jansson, L. Keene, and B. Lindberg, *Carbohydr. Res.*, **45**, 275 (1975).
(3) L. D. Melton, L. Mindt, D. A. Rees, and G. R. Sanderson, *Carbohydr. Res.*, **46**, 245 (1976).
(4) P. A. Sanford, J. E. Pittsley, C. A. Knutson, P. R. Watson, M. C. Cadmus, and A. Jeanes, *Am. Chem. Soc., Symp. Ser.*, **No. 45**, 192 (1977).
(5) R. Moorhouse, M. D. Walkinshaw, and S. Arnott, *Am. Chem. Soc., Symp. Ser.*, **No. 45**, 90 (1977).
(6) E. R. Morris, D. A. Rees, G. Young, M. D. Walkinshaw, and A. Darke, *J. Mol. Biol.*, **110**, 1 (1977).
(7) G. Holzwarth and E. B. Prestridge, *Science*, **197**, 757 (1977).
(8) G. Holzwarth, *Biochemistry*, **15**, 4333 (1976).
(9) C. Tanford, "Physical Chemistry of Macromolecules", Wiley, New York, 1961.
(10) G. Holzwarth, *Carbohydr. Res.*, **66**, 173 (1978).
(11) M. E. McDonnell and A. M. Jamieson, *J. Macromol. Sci., Phys.*, **13** (1), 67 (1977).
(12) N. C. Ford, R. Gabler, and F. E. Karasz, *Adv. Chem. Ser.*, **No. 125**, 25 (1973).
(13) P. J. Whitcomb and C. W. Macosko, *Rheology*, **22**, 493 (1978).
(14) J. G. Kirkwood and J. Riseman, *J. Chem. Phys.*, **16**, 565 (1948).
(15) T. A. King, A. Knox, W. I. Lee, and J. D. G. McAdam, *Polymer*, **14**, 293 (1973).
(16) J. L. Anderson and C. C. Reed, *J. Chem. Phys.*, **64**, 3240 (1976).
(17) W. Kuhn, *Kolloid-Z.*, **68**, 2 (1934).
(18) K. Solc and W. Stockmayer, *J. Chem. Phys.*, **54**, 756 (1971).

(19) K. Solc, *J. Chem. Phys.*, **55**, 335 (1971).
(20) M. Adam and M. Delsanti, *Macromolecules*, **10**, 1229 (1977).
(21) M. Daoud, J. P. Cotton, B. Farnoux, G. Jannik, G. Sarma, H. Benoit, R. Duplessix, C. Picot, and P. G. deGennes, *Macromolecules*, **8**, 804 (1975).
(22) P. G. deGennes, *Macromolecules*, **9**, 587 (1976).
(23) P. G. deGennes, *Macromolecules*, **9**, 594 (1976).
(24) A. M. Jamieson, L. Mack, and A. G. Walton, *Biopolymers*, **11**, 2267 (1972).
(25) W. I. Lee and J. M. Schurr, *Biopolymers*, **13**, 903 (1974).

Laser Light Scattering from Mechanically Excited Gels

R. A. Gelman[+] and R. Nossal*

National Institutes of Health, Bethesda, Maryland 20014. *Received August 9, 1978*

ABSTRACT: Laser inelastic light scattering was used to study gels which had been polymerized in light-scattering cuvettes. A sweep generator, connected to an audio frequency transducer, was used to excite mechanical oscillations in the samples. Discrete resonant peaks were noted in the voltage spectra of the scattered light at frequencies which are related to the dimensions of the cuvettes and the mechanical rigidity of the specimens. The temperature and concentration dependences of the shear modulus of elasticity were examined for several polyacrylamide gels. The data fit the relationship $\mu \sim Tc^{\alpha}$, where the exponent α has the value $\alpha \simeq 2.95$. Complementary measurements also were made when the gels were not subjected to external mechanical excitation, and the temperature and concentration dependence of the resulting Lorentzian line widths were determined.

We recently showed that laser light scattering can be used to determine elastic moduli of soft amorphous gels.[1] Standing displacement waves easily can be established within samples of such materials, as is indicated by the fact that oscillations readily appear in measured photon autocorrelation functions. The frequencies of the oscillations have been shown to depend on the dimensions of the containers and on the elastic properties of the test substance,[1] suggesting that the light-scattering cuvettes act as mechanical resonant cavities which select and enhance density fluctuations of particular wavelengths. We found that such standing waves can be sustained by weak, low-frequency, mechanical vibrations whose frequencies are not necessarily close to those of the resonant modes.

Most of our former work pertained to low-density agarose gels which move when gently shaken, and which slip easily along the sides of the light-scattering cuvettes within which they are contained.[1] In this paper, however, we report observations on cross-linked polyacrylamide samples of various compositions. Not only are these gels much stiffer than the extended agarose networks which previously were studied, but boundary conditions are different in that, when polymerized in situ, polyacrylamide gels adhere strongly to the walls of the glass cuvettes in which they are contained.

It is very difficult to observe spontaneous standing waves in such stiff, strongly adherent materials. However, when the samples are driven by an externally applied acoustic mechanical field, resonances in the self-beat light-scattering spectrum are readily apparent and measures of elasticity can be obtained. The parameter which can be extracted in this case is the shear modulus of elasticity.[2,3] Evidence to support this conclusion is presented below, where we show that values determined in the present measurements are similar to those obtained by other techniques. Moreover, changes in deduced values of moduli, which occur when temperature is varied, are shown to be in accordance with this conclusion.

Several salient aspects of the theory underlying these measurements are summarized in the next section (Techniques), where we also describe experimental procedures. In the Resonance Measurements section we present data relating to the concentration and temperature dependence of the moduli. Results of complementary line width and intensity measurements are given in the Line Width Measurements (augmenting recent work of Tanaka et al.[4]), and a short discussion appears in the Remarks section.

Techniques

a. Theory (Summary). A theoretical analysis of the cavity resonance techniques which are used in these experiments is presented in detail in ref 2. The model adopted therein relates fluctuations in the diffraction pattern of scattered light to the reorganization of a polymer lattice which occurs when a macroscopic displacement wave passes through an isotropic gel. The details of the diffraction pattern cannot be specified unless the microscopic structure of the gel has been determined, but we nevertheless know that the scattering pattern will vary with the same temporal periodicity as will macroscopic displacements which might be induced in the material. Gels having high polymer concentration may, to first order, be spatially homogeneous on a length scale comparable to the wavelength of light, but scattering from imperfections such as domain boundaries and dust will produce a weak, time-varying, diffraction pattern. Moreover, if the polymer concentration is sufficiently low (as, e.g., in the agarose and fibrin gels which we have reported on elsewhere[1,5]), spatial heterogeneities intrinsic to the gel structure itself will exist on a length scale of the order of that of light, and a larger amount of scattering will be discerned.

To describe macroscopic motions we assume[2] that the following modified classical elasticity equations can be used:

$$\rho \frac{\partial^2 U_{x_i}}{\partial t^2} = \mu \nabla^2 U_{x_i} + (\lambda + \mu) \frac{\partial}{\partial x_i} (\nabla \cdot \mathbf{U}) + \varphi_{x_i} - \zeta \left(\frac{\partial U_{x_i}}{\partial t} - V_{x_i} \right) + \eta \nabla^2 \frac{\partial U_{x_i}}{\partial t} + (\chi + \eta) \frac{\partial}{\partial x_i} \left(\nabla \cdot \frac{\partial \mathbf{U}}{\partial t} \right) \quad (1)$$

In these equations $\mathbf{U}(\mathbf{r},t) \equiv (U_x, U_y, U_z)$ are the components of the displacement vector, ρ is the material density, λ and

* Physical Sciences Laboratory, DCRT.
[+] Laboratory of Biochemistry, NIDR.